ELSEVIER

Polymer 40 (1999) 4169–4180

polymer

X-ray scattering studies of orientation in channel flows of a lyotropic liquid crystalline polymer

David K. Cinader Jr, Wesley R. Burghardt*

Department of Chemical Engineering, Northwestern University, Evanston, IL 60208, USA

Received 6 May 1998; received in revised form 15 August 1998; accepted 1 September 1998

Abstract

A lyotropic solution of hydroxypropylcellulose in *m*-cresol has been studied in channel flows containing inhomogeneous shearing kinematics (planar Poiseuille), or mixed shearing and extensional kinematics (slit-contractions and expansions). We have used X-ray scattering as a probe of orientation, to test and extend previous birefringence measurements in the same system [Bedford BD, Burghardt WR. J Rheol 1996;40:235]. Orientation changes dramatically in contraction and expansion regions, which cannot be explained by changes in superficial velocity alone. Calculations using Ericksen's Transversely Isotropic Fluid model show that the addition of a modest amount of extension to otherwise shearing kinematics can influence alignment by perturbing tumbling orbits either into or out of the shear plane, in addition to inducing a transition from tumbling to flow aligning behavior. Away from the centerline, orientation is rotated away from the downstream direction, presumably due to streamline bending near the contraction and expansion. However, the degree of rotation is different in contraction and expansion flows.

Keywords: Channel flows; Liquid-crystalline polymer; Molecular orientation

1. Introduction

Due to the spontaneous local alignment of rigid-rod molecules even in the quiescent state, flow fields are able to impart tremendous orientation in liquid-crystalline polymers (LCPs). This can be beneficial in structural applications where high orientation can result in enhanced mechanical properties. However, high orientation can be deleterious when isotropic properties are desired. In either case, understanding of how orientation develops in response to flow fields during processing will aid in the design of effective products.

Uniaxial extension encountered during fiber spinning clearly promotes molecular orientation along the fiber axis, leading to exceptional tensile strength and stiffness in fibers spun from LCP melts and solutions. Because the solvent must be removed during processing, commercial technology of lyotropic LCPs is limited to fiber spinning. Conversely, thermotropic LCPs may also be extruded and injection molded. In these processes, flow fields typically involve mixtures of shear and extension, and the resulting orientation state is much more difficult to anticipate.

Many investigators have sought to understand the effects of flow on orientation in thermotropes [1–11]. However, most have examined finished products in the solid state, making it difficult to separate the effects of the flow field from those due to the transient, nonisothermal nature of injection molding. In this work, our objective is to use in situ methods to isolate the effects of complex kinematics in mixed shear and extensional flows on the molecular orientation state in LCPs. Our group has developed several methods for in situ measurements of molecular orientation in lyotropes under flow. In simple shear, we have used both flow birefringence [12–14] and X-ray scattering [15] for this purpose. Bedford et al. extended the birefringence technique to investigate inhomogeneous shear flow [16,17] and mixed shear and extensional flow [18] of model lyotropic LCPs. Here we test and extend these measurements using in situ X-ray scattering.

There are several motivations for applying X-ray scattering to this problem. Our ultimate objective is development of in situ techniques for studying orientation development in commercial thermotropes. Since these materials are typically opaque, X-ray methods are quite suitable where optical techniques fail. The present work on lyotropes is an intermediate step towards this ultimate goal. The second motivating force is that X-ray scattering provides a more direct probe of orientation than birefringence. While our

* Corresponding author. Tel.: + 1-847-467-1401; Fax: + 1-847-491-3728.

E-mail address: w-burghardt@nwu.edu (W.R. Burghardt)

0032-3861/99/$ - see front matter
PII: S0032-3861(98)00667-3

previous work in simple shear has demonstrated that birefringence usually provides a reliable measure of bulk orientation, it can possibly fail due to complications associated with how the polarization of light is affected by spatially inhomogeneous media [15]. In a similar vein, we have reported anomalies in the interference colors observed between crossed polarizers in channel flows of lyotropes, which are attributed to spatial variation of the macroscopic optical axis of the fluid as light passes through the sample [17]. As flow fields—and the resulting orientation state—become more complex, interpretation of birefringence measurements as a measure of average orientation becomes more tenuous. In this regard, the present work provides an independent test of the conclusions of our previous birefringence studies [16,18]. Finally, X-ray scattering provides a more complete picture of the orientation distribution as compared with birefringence or optical absorption spectroscopy (dichroism), which provide measures of only the second moment of the distribution function.

A basic factor in considering how flows influence molecular orientation in lyotropic LCPs is the known fact that they exhibit *director tumbling* [19]. That is, hydrodynamic torques in shear flows act to rotate the nematic director rather than to promote steady flow alignment. In general, tumbling in shear acts to generate a textured orientation state with a high density of defects, although some net orientation is produced [12–15]. Tumbling dynamics may be explored in the context of Ericksen's Transversely Isotropic Fluid model [20], wherein the propensity for a material to tumble is described by a single parameter, λ. Values of λ less than 1 lead to tumbling in shear, while values greater than 1 lead to flow aligning behavior, where the director lies within the shear plane at some constant angle relative to the flow direction. Regardless of the tendency towards tumbling in shear, *extensional* flows always act to promote steady alignment along the extension axis. In mixed shear/extensional flows of the sort likely to be encountered in molding and extrusion, the competition between these tendencies will largely determine the resulting orientation state.

In their birefringence studies in slit contraction flows, Bedford and Burghardt [18] observed strong enhancement in orientation, which they attributed to a transition from tumbling to flow aligning dynamics induced by extension. Using the Ericksen model, they showed that a modest amount of extension could lead to such a transition. However, in order to generate such a transition in a significant fraction of the flow, they had to assume values of the tumbling parameter, λ, that were unrealistically close to unity. We begin this paper with a more complete analysis using the Ericksen model to gain insights into how added extension might influence orientation dynamics in complex flows of LCPs.

2. Analysis

Ericksen's Transversely Isotropic Fluid model includes an evolution equation for the director, **n**, and an orientation-dependent constitutive relationship between the stress and deformation. Here, we focus on the evolution equation which is written as:

$$\frac{D\mathbf{n}}{Dt} = \mathbf{n}\cdot\boldsymbol{\Omega} + \lambda(\mathbf{n}\cdot\mathbf{D} - \mathbf{D} : \mathbf{nnn}) \tag{1}$$

D and **Ω** are, respectively, the rate of deformation and vorticity tensors, which contain the information about the imposed flow kinematics. The flow fields considered in our work are slit flows in which there is a superimposed contraction or expansion in the channel cross section [18]. Along the centerline of these flows, the kinematics may be broken down into a shearing deformation (in which '1' represents the flow direction, '2' represents the shear gradient direction and '3' represents the vorticity direction), and a planar extensional flow with its extension and compression axes along the 1 and 3 axes (that is, the superimposed extensional flow involved stretching *orthogonal* to the shear plane) [18] For these kinematics:

$$\mathbf{D} = \frac{\dot\gamma}{2}\begin{bmatrix} 2\rho & 1 & 0 \\ 1 & 0 & 0 \\ 0 & 0 & -2\rho \end{bmatrix} \quad \boldsymbol{\Omega} = \frac{\dot\gamma}{2}\begin{bmatrix} 0 & -1 & 0 \\ 1 & 0 & 0 \\ 0 & 0 & 0 \end{bmatrix} \tag{2}$$

where

$$\rho = \frac{\dot\varepsilon}{\dot\gamma}$$

Here ρ gives the relative importance of extension to shear, and $\dot\gamma$ is the shear rate. These two variables will vary as a function of position; for instance, in slit flows, $\dot\gamma$ varies from zero at the midplane to a maximum at the walls. Although analyses based on these kinematics will be locally valid, it is also necessary to account for the variation of these parameters as a function of position within a slit contraction or expansion flow to develop a picture of how the macroscopic orientation state will evolve [18]. Positive values of ρ indicate stretching along the 1-direction, and would be developed in a slit contraction flow. Conversely, negative values of ρ indicate stretching along the 3-direction, and would be generated in a slit expansion flow.

For these kinematics, the director evolution equations become:

$$\frac{dn_1}{dt} = n_2\frac{\dot\gamma}{2} + \lambda\frac{\dot\gamma}{2}\left(2\rho n_1 + n_2 - 2\rho n_1^3 - 2n_1^2 n_2 + 2\rho n_1 n_3^2\right) \tag{3}$$

$$\frac{dn_2}{dt} = -n_1\frac{\dot\gamma}{2} + \lambda\frac{\dot\gamma}{2}\left(n_1 - 2\rho n_1^2 n_2 - 2n_2^2 n_1 + 2\rho n_2 n_3^2\right) \tag{4}$$

$$\frac{dn_3}{dt} = \lambda\frac{\dot\gamma}{2}\left(-2\rho n_3 - 2\rho n_1^2 n_3 - 2n_1 n_2 n_3 + 2\rho n_3^3\right) \tag{5}$$

In our analysis, we first seek steady solutions by setting the time derivatives equal to zero. The stability of these

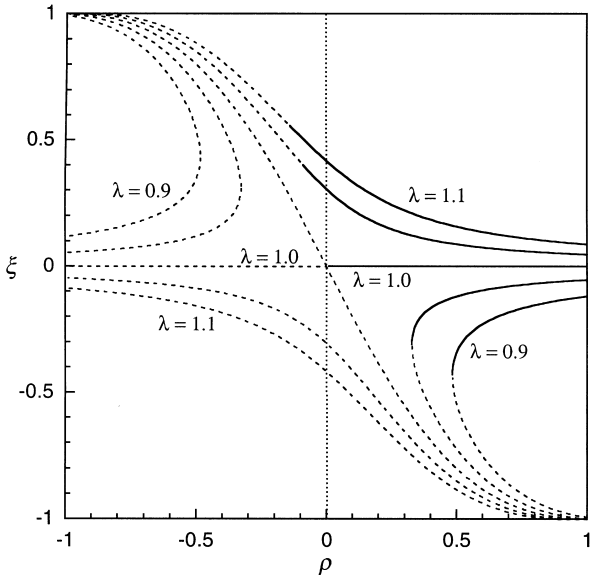

Fig. 1. Steady in-plane solutions to the Leslie–Ericksen director evolution equations: $\xi = \sin(2\theta)$ vs relative importance of extension to shear, ρ. Dashed lines indicate unstable solutions, while solid lines indicate stable solutions, for the following values of tumbling parameter: $\lambda = 0.9$, 0.95, 1.0, 1.05, and 1.1. Shear flow conditions ($\rho = 0$) are denoted by the dotted line.

solutions is then explored by a standard linear stability analysis, linearizing the right-hand side of the director evolution equations about the steady solutions. The eigenvalues of the coefficient matrix then reveal the stability of the solutions.

We first consider the steady solutions for which the director lies along the vorticity direction, $\mathbf{n} = [0,0, \pm 1]$. In simple shearing flow ($\rho = 0$) when $\lambda < 1$ this steady state is marginally stable; small perturbations lead to a periodic response that neither decays nor grows (this reflects unperturbed tumbling dynamics in shear). With mixed shear/extensional kinematics and $\lambda < 1$, stability analysis yields the following conditions:

$$\rho < 0 \text{ and } \rho^2 > \frac{1-\lambda^2}{\lambda^2} \text{ stable node}$$

$$\rho < 0 \text{ and } \rho^2 < \frac{1-\lambda^2}{\lambda^2} \text{ stable spiral}$$

$$\rho > 0 \text{ and } \rho^2 < \frac{1-\lambda^2}{\lambda^2} \text{ unstable spiral}$$

$$\rho > 0 \text{ and } \rho^2 > \frac{1-\lambda^2}{\lambda^2} \text{ unstable node}$$

These conditions show that the addition of extension along the 3-axis (negative ρ) acts to stabilize vorticity-alignment of the director, while addition of extension along the 1-axis (positive ρ) leads to destabilization.

We have also examined the behavior for $\lambda > 1$ (i.e., a flow-aligning nematic). In simple shear ($\rho = 0$), vorticity alignment is unstable. If this steady state is perturbed, the director will seek out and find the stable flow aligned state within the 1–2 plane (see below). With mixed shearing and extension, for $\lambda > 1$ we find:

$$\rho < 0 \text{ and } \rho^2 > \frac{\lambda^2-1}{8\lambda^2} \text{ stable node}$$

$$\rho < 0 \text{ and } \rho^2 < \frac{\lambda^2-1}{8\lambda^2} \text{ unstable saddle}$$

$$\rho > 0 \text{ and } \rho^2 < \frac{\lambda^2-1}{8\lambda^2} \text{ unstable saddle}$$

$$\rho > 0 \text{ and } \rho^2 > \frac{\lambda^2-1}{8\lambda^2} \text{ unstable node}$$

Addition of extension along the 1-axis ($\rho > 0$) further destabilizes vorticity alignment of a flow aligning nematic. Conversely, addition of extension along the 3-axis ($\rho < 0$) can lead to stabilization of this steady vorticity alignment, provided that $|\rho|$ exceeds some threshold value.

We now consider steady solutions that lie within the 'shear' plane ($n_3 = 0$). Eq. (3) and Eq. (4) reduce to a nonlinear equation for $\xi = \sin(2\theta)$, where $n_1 = \cos\theta$ and $n_2 = \sin\theta$:

$$1 + \lambda\rho\xi - \lambda\sqrt{1-\xi^2} = 0 \tag{6}$$

which may be solved for ξ:

$$\xi = \frac{-2\lambda\rho \pm \sqrt{(2\lambda\rho)^2 - 4(\lambda^2\rho^2 + \lambda^2)(1-\lambda^2)}}{2(\lambda^2\rho^2 + \lambda^2)} \tag{7}$$

These steady solutions are plotted in Fig. 1 for various values of λ, including both tumbling and flow aligning nematics. The stability of these solutions was examined by calculating the eigenvalues of the coefficient matrix described above. Unstable solutions are designated by the broken lines in Fig. 1.

In simple shear flow ($\rho = 0$), two steady solutions exist for flow aligning nematics ($\lambda > 1$). Of these, the solution in the first quadrant of the 1–2 plane is stable, corresponding to the standard flow alignment orientation in shear. Following this stable flow-aligned solution branch, the steady state value of ξ decreases as extension is added along the 1-axis (positive ρ), indicating that the director becomes more closely aligned with the 1-axis. Conversely, in the presence of extension along the 3-axis, the steady flow alignment solution remains stable up to some threshold, and then becomes unstable. This occurs at the same (negative) value of ρ at which vorticity alignment becomes stable (see above).

This abrupt transition in stable alignment states leads to an interesting prediction for a flow-aligning nematic in the diverging region of a slit-expansion flow. At the midplane, the shear rate is zero, which means that $|\rho|$ becomes infinite. Here, stretching along the 3-axis leads to stable vorticity alignment. Conversely, the extension goes to zero at the walls, while the shear rate will be maximum, leading to $\rho = 0$ and the standard shear flow alignment condition. As one moves from the walls to the midplane, there will always

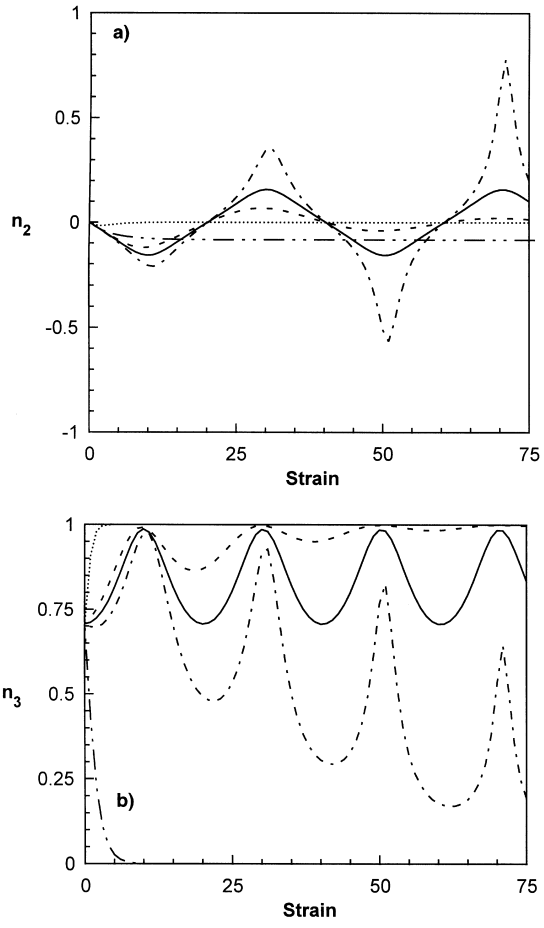

Fig. 2. Simulations of the evolution of director components under mixed shear/extensional flow for $\rho = -0.4$ (· · ·), -0.02 (- - - -), 0 (————), 0.02 (— – —) and 0.4 (— – – —). (a) n_2 vs strain. (b) n_3 vs strain.

be some location at which the stable orientation state switches from the in-plane solution, given in Fig. 1, to vorticity alignment. X-ray measurements of orientation in which the beam passes through the full sample thickness should thus reveal two discrete populations of orientation, one aligned within the shear plane and the other along the vorticity direction.

Turning now to the case of tumbling materials with $\lambda < 0$, we first note that no steady-state solution exists in shear flow ($\rho = 0$). While *steady* solutions may be generated by adding sufficient extension along either the 1- or 3-axes, the only *stable* solution results from adding stretching along the 1-axis ($\rho > 0$).

Bedford and Burghardt [18] observed dramatic enhancements in alignment following a contraction in channel flow. They attributed this to a transition from tumbling to flow aligning behavior brought about by the extensional character of the flow, as predicted in Fig. 1. Along the midplane, where the shear rate goes to zero, any amount of extension will induce a flow-aligned condition. However, in the slit contractions studied by Bedford and Burghardt, measurements of kinematics showed that the superimposed extension was fairly weak; as one moves away from the midplane towards the walls, $|\rho|$ rapidly becomes small. In order for a substantial fraction of the flow field to undergo an extension-induced transition to flow alignment, Bedford and Burghardt had to assume a value of $\lambda = 0.998$, which is unreasonably close to 1.

We believe that this paradox may be resolved by considering what happens to tumbling dynamics when ρ is positive (which would be the case *throughout* a slit-contraction flow), but insufficiently large to induce the transition to flow alignment seen in Fig. 1. To this end we have undertaken simulations of the director evolution Eqs. (3)–(5) using a realistic tumbling value of $\lambda = 0.95$, for various values of ρ. Fig. 2 shows the evolution of the resulting director components as a function of strain, where the initial condition lies intermediate between the shear plane and the vorticity axis. For simple shearing kinematics ($\rho = 0$) persistent tumbling is predicted, with no drift of the tumbling orbit towards either the shear plane or vorticity direction. When ρ is negative, the tumbling orbit either drifts or is immediately drawn towards vorticity alignment ($n_3 = 1$), as would be anticipated from the stability analysis above. When ρ is sufficiently positive, the director is immediately drawn to the stable in-plane solution predicted in Fig. 1. When ρ is less positive, the added extension is insufficient to lead to a stable flow aligned solution. However, because of the added extension, the tumbling orbits tend to drift into the shear plane, so n_3 decreases while $|n_1|$ and $|n_2|$ increase with applied strain. Note that the value of $\rho = 0.02$ used in this calculation represents a very slight amount of added extension, and is well below the value needed to induce alignment. This attraction of tumbling orbits to the shear plane will lead to a significant net enhancement in orientation, even though tumbling is not suppressed. This is a much less demanding criterion than the one applied by Bedford and Burghardt [18] and it seems likely that a significant portion of the enhancement of orientation observed in their experiments was due to this effect rather than an extension-induced flow-aligned state per se. (Of course, at the midplane in a slit-contraction flow, extension will *always* lead to a steady aligned state.)

3. Experiment

3.1. Materials

A 27% solution of hydroxypropylcellulose (HPC) in *m*-cresol was used in this investigation. The HPC has a nominal M_w of 80 000. This sample has previously been studied by Bedford and coworkers using birefringence in channel flows [17,18] and by Hongladarom and workers using X-ray scattering and birefringence in homogeneous shear flow [15]. We will be making comparisons with the previously published birefringence data of Bedford and

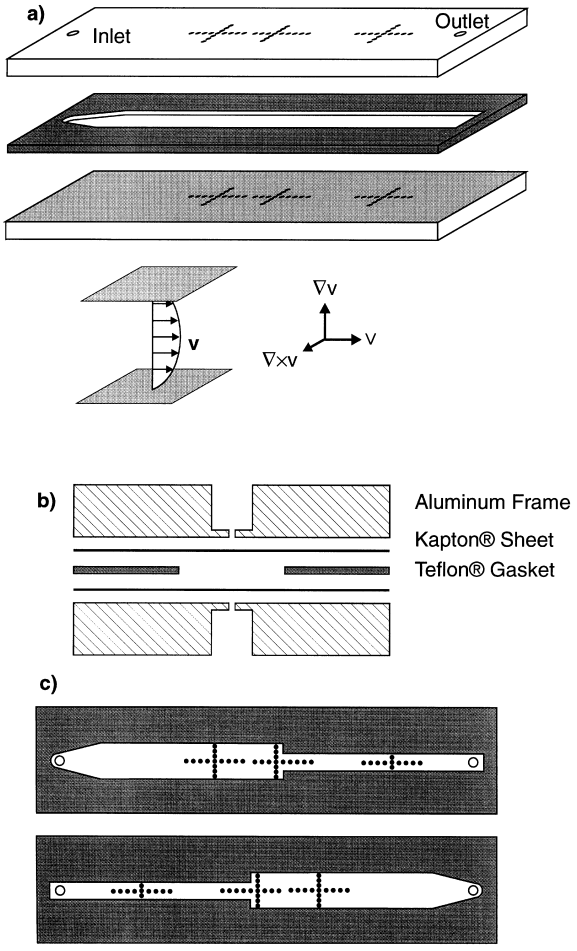

Fig. 3. Schematic of the flowcell used in X-ray scattering experiments. (a) View showing the Teflon® spacer sandwiched between the two aluminum frames. Also shown is a schematic illustrating the velocity (**v**), gradient (**∇v**) and vorticity (**∇x v**) directions characterizing the inhomogeneous shear flow expected in the plane Poiseuille geometry away from the edges of the spacer. (b) Exploded cross-section (end view) showing the Kapton® sheets supported by the aluminum frames. (c) Diagrams of the slit flow channels for 2:1 contraction and 1:2 expansion showing the points available to the X-ray beam.

Burghardt [18]; these data were obtained using a spectrographic technique introduced by Hongladarom et al. [12] The reader is referred to these sources for details of the birefringence experiments.

3.2. X-ray scattering measurements

Measurements of orientation in simple shearing flows using birefringence and X-ray scattering were reported by Hongladarom et al. [15] Experiments on several model lyotropes showed that birefringence measurements yield information proportional to the X-ray scattering orientation parameter. For the case of the 27% solution of HPC in *m*-cresol studied here, the relationship was found to be:

$$\Delta n = 0.0035S \tag{8}$$

We will use this equation to convert the effective birefringence previously measured in nonhomogeneous flows [18] to an effective orientation parameter, representing the degree of orientation averaged through the thickness of our slit flow (see below).

To perform in situ X-ray measurements in channel flows, we used the same recirculating system for pumping the fluid as in the birefringence experiments of Bedford and Burghardt [16–18], but constructed a new flow cell. A redesigned set of aluminum frames and thin (50 μm) Kapton® sheets replaced the aluminum frames and glass windows used previously. Diagrams of the flow cell are shown in Fig. 3. The Kapton® sheets were used as window material to reduce the amount of radiation lost to absorption. Owing to the high pressures generated in circulating the viscous fluid, the Kapton® sheets were supported by the aluminum frames, through which an array of trenches and holes were cut to allow transmission of the incident and scattered X-ray beam. Fig. 3b shows a cross-section illustrating how these holes allow X-ray access. The channel geometries were determined by the same interchangeable Teflon® spacers used in our optical flow cell. These define a flow channel with thickness = 1/16″ and width = 1″. Thus, for most of the channel, the dominant velocity gradient lies normal to the windows. Fig. 3c illustrates the spacer used for 2:1 slit-contraction and 1:2 slit-expansion flows, indicating the locations in the flow with X-ray access through the holes in the aluminum frames. A nickel-filtered copper tube X-ray generator was used to produce 8 keV radiation. Image plates were used to record two dimensional X-ray scattering patterns, with exposure times of 10–15 min.

4. Interpretation of the orientation parameter

4.1. X-ray scattering as a measure of orientation

We have followed the procedure for quantifying orientation described by Mitchell and Windle [21]. They define a molecular order parameter, S_m, as the coefficient of the second term in a Legendre series representation of the orientation distribution function of the rodlike molecules. If *s* is the magnitude of the scattering vector and α is the azimuthal angle, then S_m is determined from a 2-D X-ray scattering pattern by computing the average of P_2 weighted by the measured azimuthal intensity scan, and dividing this by the value expected for a system in which the rod-like molecules are perfectly oriented along the director (α = 0). This leads to:

$$S_m = \frac{\langle P_2(\cos\alpha)\rangle}{\langle P_2(\cos\alpha)\rangle_0} = -2\frac{\int_0^{\pi/2} I(s,\alpha)P_2(\cos\alpha)\sin\alpha d\alpha}{\int_0^{\pi/2} I(s,\alpha)\sin\alpha d\alpha} \tag{9}$$

S_m ranges from 1 for perfect alignment in the α = 0 direction to zero when the orientation distribution (and scattering pattern) is isotropic. $P_2(\cos\alpha)$ is the second

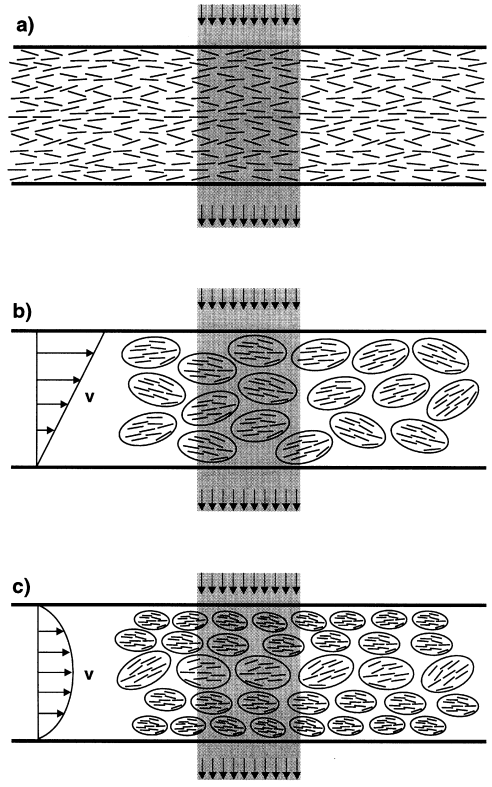

Fig. 4. Schematic of various scattering situations. Shaded area denotes regions illuminated by X-ray beam. (a) Monodomain. (b) Homogeneous shearing of a sample with texture. (c) Pressure-driven flow of a sample with texture. Note that the molecules and the 'domains' are not drawn to scale with the experimental geometry nor with the X-ray beam.

Legendre polynomial, and $I(s, \alpha)$ is the azimuthal intensity distribution. To capture information about the strength of the nematic orientation distribution, we scan the azimuthal intensity at a value of the scattering vector corresponding to the intermolecular correlation distance, revealed by a peak observed as a function of scattering vector, *s*. To account for variations in exposure and image plate sensitivity, each scan is normalized by dividing by its own area. In addition, the shadow of the beamstop holder is removed from the azimuthal scan. To remove the effects of extraneous isotropic scattering due to air, windows, solvent, etc., a single constant background value is chosen and subtracted from each normalized azimuthal scan prior to computing the orientation parameter using Eq. (9). The choice of this constant will be discussed in a later section.

The analysis leading to Eq. (9) assumes a uniaxial distribution of molecular orientation about the director, and neglects the possible presence of a 'polydomain' texture. These conditions would be appropriate, for instance in a nematic monodomain, as illustrated in Fig. 4a, in which case such measurements should yield a direct measure of the molecular order parameter S_m. The rigor of this interpretation is compromised by the somewhat arbitrary choice of baseline [15,21], and the lack of precise knowledge about the scattering pattern which would result from perfect orientation of the molecules (Mitchell and Windle assume perfectly rigid, infinitely long rods, which would produce a delta function at $\alpha = \pi/2$ in the azimuthal scan [21]).

4.2. Application to homogeneous flows of textured LCPs

In reality, LCPs under shear do not typically exist as monodomains but rather have a heterogeneous distribution of director orientation with 'domains' of sizes on the order of microns. When a 2-D scattering pattern collected under these circumstances is analyzed according to Eq. (9) above, we refer to the result as an 'orientation' parameter. Interpretation of an orientation parameter from a textured sample requires recognition that distributions of orientation exist at two levels. At the molecular level, S_m describes the degree of orientation around the local director. The texture may be conceptualized in terms of a distribution of *director* orientations, with an associated texture order parameter, S_{text}. Since scattering patterns are produced by the sum of contributions from each molecule in the illuminated sample, they simultaneously represent both texture and molecular orientation distributions, as illustrated in Fig. 4b. (This is a conceptual illustration, and not intended to faithfully represent LCP structure under shear, which is far more complex [22]. Rather, we wish simply to convey the concept that the measured orientation reflects averages over two levels of structure.) The measured orientation parameter may be thought of as: $S = S_m \cdot S_{text}$, recognizing both distributions in orientation.

4.3. Application to nonhomogeneous flows

Pressure-driven channel flows present an additional level of complexity. Here, the flow field involves varying stress levels and deformation histories, and hence fluid structure, as one traverses from one wall to the other. The orientation state will be a function of depth in the fluid. The sampling of the structure in such a situation is shown schematically in Fig. 4c. The orientation parameter measured under these circumstances is an average of the orientation states encountered as the X-ray beam passes through the flow field thickness:

$$S_{eff} = \frac{1}{h}\int_0^h S_{text}(x)\, S_m(x) dx \tag{10}$$

This is justified on the basis that each fluid element through which X-rays pass contributes equally to the scattering. The effective orientation parameter, S_{eff}, reflects an average over the flow cell thickness.

In the special case of slit flow (a nonhomogeneous shear flow), Bedford and Burghardt [16,18] have shown that the average orientation, as measured by birefringence, may be predicted from independent measurements of orientation in simple shearing flow. This rests on the fact that the integral in Eq. (10) may be converted to an integral over shear stress (since stress varies linearly with position in slit flow), and the hypothesis that the local fluid structure at a particular

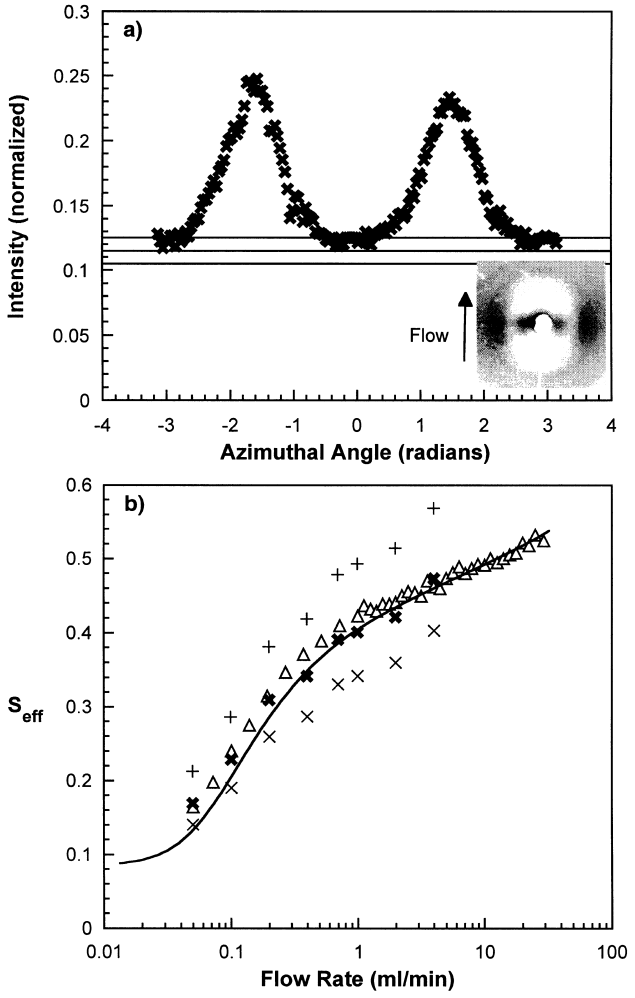

Fig. 5. Effect of choice of background scattering level on the computed orientation parameter in slit flow. (a) Comparison of background values of 0.105, 0.115, and 0.125 with the normalized azimuthal scan taken in contraction flow at a high flow rate (these conditions should minimize polymer scattering along the meridian. (b) Orientation parameters calculated from X-ray scattering data in slit flow using the following values of the background scattering: (×) 0.105, (✖) 0.115, and (+) 0.125. Birefringence data from Bedford and Burghardt [16] are represented by triangles (△), while the solid line denotes predictions of orientation in slit flow based on measurements in simple shear flow, Eq. (11).

depth in slit flow is the same as would be present in simple shear at the same stress level. Making this transformation, the effective orientation parameter in slit flow may be predicted by:

$$S_{\text{eff}} = \frac{1}{\tau_w}\int_0^{\tau_w} S(\tau)d\tau \tag{11}$$

5. Results

In situ X-ray scattering experiments were performed in the channel flow for three different configurations: planar Poiseuille, 2:1 slit-contraction, and 1:2 slit-expansion. Results will be presented sequentially for each case.

5.1. Plane Poiseuille (slit) flow

We first address the issue of identifying a suitable background value to subtract from the azimuthal scans of scattered intensity. In the homogeneous shearing flows studied by Hongladarom et al. [15] this was chosen as the lowest value of the intensity observed in all of the experiments for a given sample, which turns out to be that corresponding to the highest shear rate. The assumption is that at the highest shear rate, molecular orientation is maximized along the flow direction, leading to a concentration of scattering on the equator. Assuming there are no molecules remaining oriented along the vorticity axis, there should be no polymer contribution to scattering along the meridian where the minimum in scattered intensity is found.

For the pressure-driven flows studied here, the baseline was similarly chosen as the lowest value of the intensity in the experiment expected to give the greatest orientation. This was found to be an image collected at the contraction in 2:1 contraction flow at the highest flow rate studied. Fig. 5a shows the normalized azimuthal intensity scan of this image. Since there is some noise in the data (these experiments produced noisy images with substantial background scattering), we have investigated three possible choices for background values to be subtracted, as indicated.

Fig. 5b illustrates the consequences of choosing different background values in analyzing effective orientation parameter measured in slit flow as a function of volumetric flow rate. Lower background values lead to lower S_{eff}, while higher background values lead to higher S_{eff}. Of the three background values, the middle one (a value of 0.115) most faithfully reproduces the procedures used in our previous homogeneous shear flow experiments comparing X-ray and birefringence measurements of orientation [15]. Using the relationship between orientation parameter and birefringence found in that experiment [Eq. (8)], we may convert the slit flow birefringence data of Bedford and Burghardt [18] and compare to these X-ray scattering results. Not surprisingly, the background value of 0.115 also leads to a favorable comparison between these X-ray and birefringence data in nonhomogeneous shear. Thus, for the remainder of our data analysis, this baseline value will be used. These results illustrate how the exact values of S reported in these kinds of experiments are influenced by choices such as background subtraction procedures. However, rigorous adherence to this procedure is effective in allowing self-consistent calculation and reporting of the orientation induced under varying flow conditions.

Bedford and Burghardt [16,18] confirmed that measurements of orientation in simple shearing experiments could be used to predict the orientation in a pressure-driven slit flow, thus supporting the hypothesis that the structure of a

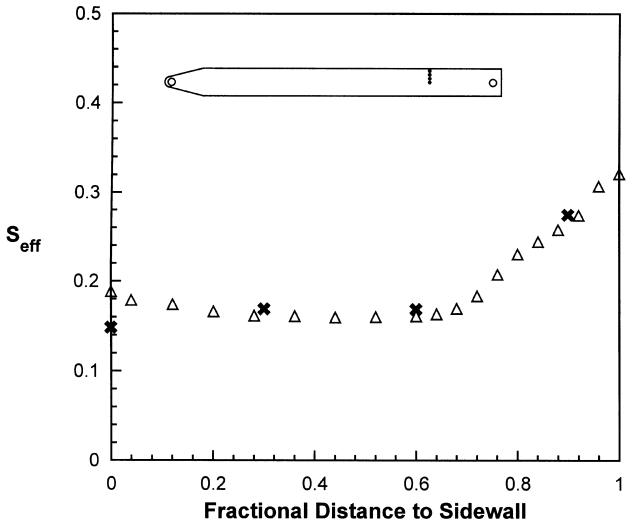

Fig. 6. Orientation as a function of proximity to the sidewall in slit flow for a flow rate of 0.05 ml.min^{-1}. (✖) X-ray scattering and (△) birefringence. Filled circles on the schematic of the flow field indicate positions at which data were taken.

fluid element is determined only by its own local stress and deformation history. The solid curve in Fig. 5b illustrates this by predicting the effective orientation parameter according to Eq. (11), using homogeneous shear flow data for S as a function of shear stress level [18]. At flow rates of around 0.5 ml.min^{-1} and above, an instability in fluid structure sets in, leading to time-dependent birefringence signals [17,18]. Given the long exposure times used here, these X-ray measurements of orientation will average over these small fluctuations in average orientation.

Cross-channel measurements of the orientation parameter taken 25 cm downstream of the inlet at a flow rate of 0.05 ml.min^{-1} are shown in Fig. 6. Strong enhancements in orientation are observed near the sidewall. This corroborates the birefringence findings of Bedford and Burghardt [18], which are converted to S_{eff} in Fig. 6 using Eq. (8).

5.2. Slit-contraction flow

Measurements of orientation were taken along the centerline in 2:1 slit-contraction flow for flow rates of 0.1 and 1.0 ml.min^{-1}. Fig. 7 shows dramatic increases in orientation upon contraction and subsequent decay downstream of the contraction. This increase is much larger than expected based on the two-fold increase in superficial velocity in the downstream slit flow section (which may be predicted using Eq. (11)). This leads us to conclude that the extensional component of the flow is responsible. The decay of orientation after the contraction occurs much more slowly, presumably being driven by the shear-induced tumbling downstream of the contraction where extension is no longer present. Previous birefringence data of Bedford and Burghardt collected under identical flow conditions have been converted to S_{eff} using Eq. (8), and, again, there is excellent agreement between these two techniques for quantifying LCP orientation under flow.

As mentioned in the introduction, twisting of the orientation of the LCP with depth in the flow cell can lead to anomalous effects on light polarization [17]. Such effects are more likely to occur in slit expansions and expansions away from the centerline, where bending of the streamlines and possibly unfavorable extensional gradients will induce rotation of orientation away from the downstream direction. Under these circumstances, X-ray scattering provides a much more reliable way to measure both the degree and direction of the average molecular orientation.

Rotation of the average orientation direction away from the prevailing flow direction is manifested by a twisting of the 2D X-ray scattering pattern away from the flow direction, as is illustrated in Fig. 8a. The amount of rotation was quantified by using the azimuthal intensity distribution to calculate an intensity sum weighted by an odd function:

$$\sum(\chi) = \int_{\chi-\pi/2}^{\chi+\pi/2} I(\alpha)\,\mathrm{sgn}(\alpha-\chi)\,d\alpha \tag{12}$$

$\Sigma(\chi)$ will vanish at four points: the two peaks and the two valleys of the azimuthal distribution $I(\alpha)$. The displacement of these zeros from 0, $\pm\,\pi/2$ and $\pm\,\pi$ then reveals the amount of rotation away from the downstream direction, which we take to be a measure of the average orientation angle of the LCP. This procedure is illustrated in Fig. 8b and c. The orientation parameter in these cases is then calculated by redefining $\alpha = 0$ in Eq. (9) to correspond to one of the valleys in orientation.

Fig. 9 presents measurements of orientation parameter and orientation direction measured across the width of the channel at an axial location 0.75 cm upstream of the contraction. Near the centerline, the orientation parameter is significantly enhanced due to the addition of extension in the contraction region. Fig. 9b reports the amount of rotation in LCP orientation away from the downstream direction, quantified using the method described above. The sense of the rotation indicates that the local orientation tracks the streamlines as they bend into the contraction. Owing to symmetry, the rotation angle passes through zero along the centerline. Near the side walls, the orientation returns close to the downstream direction, so that the maximum rotation of the orientation occurs midway between the centerline and sidewalls.

5.3. Slit-expansion flow

Measurements of orientation along the centerline in 1:2 slit-expansion flow show a dramatic decrease in orientation followed by a subsequent recovery. This is shown in Fig. 10 for flow rates of 0.1 and 1.0 ml.min^{-1}. As in the contraction experiments, this decrease is much larger than would be expected based on changes in superficial velocity alone in nonhomogeneous shear, indicating that the superimposed

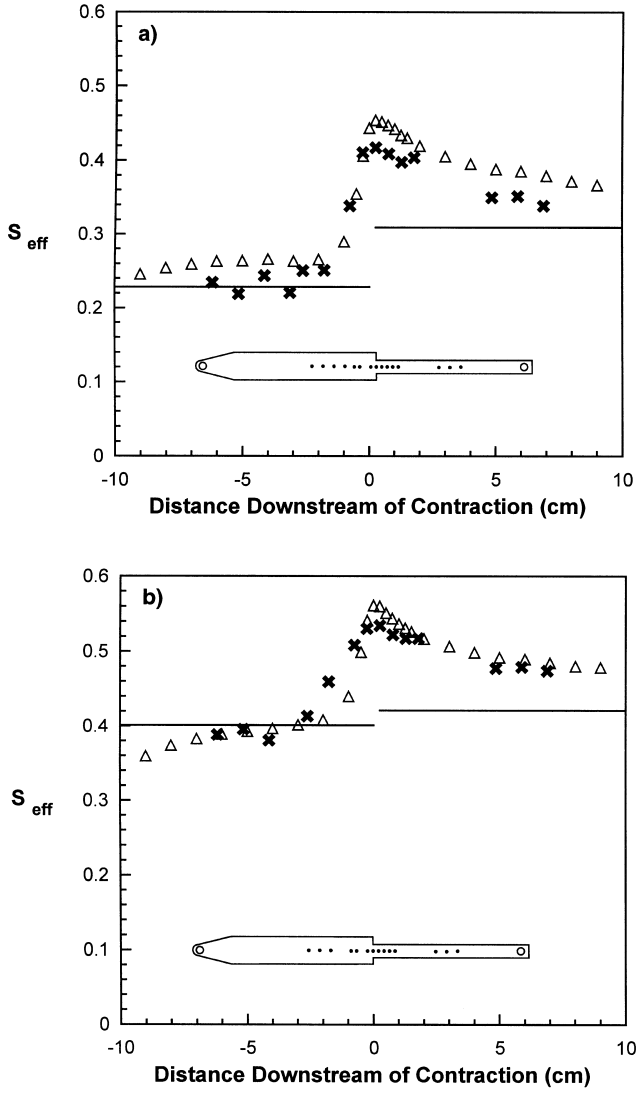

Fig. 7. Centerline orientation in contraction flow for rates of (a) 0.1; and (b) 1.0 ml.min^{-1}. (✖) X-ray scattering and (△) birefringence. Lines denote predictions of orientation in inhomogeneous shear based on flow rate alone. Filled circles on the schematic of the flow field indicate positions at which data were taken.

extension (in this case acting transverse to the downstream direction) has a strong influence on the orientation state.

Cross-channel measurements of orientation taken 0.75 cm downstream of the expansion are shown in Fig. 11. At this axial location, the centerline orientation has not yet dropped to its lowest point under the influence of the diverging channel (see Fig. 10a), but the effects of the diverging channel are strongly felt away from the centerline where even lower values of orientation parameter are observed. Somewhat surprisingly, the orientation rebounds to a very high value near the two side walls.

The mean orientation direction is determined as described above, and is reported in Fig. 11b. Qualitatively, the mean orientation shows a rotation away from the downstream direction which is consistent with that expected based on divergence of streamlines in the expansion region. However, the maximum degree of rotation of the LCP orientation is significantly lower in the expansion flow than in the contraction flow, despite the similarity in geometry and measurement location.

6. Discussion

6.1. Planar Poiseuille flow

Results of effective orientation parameter as a function of volumetric flow rate in Fig. 5 further reinforce the predictive power of the local response hypothesis, previously tested by Bedford and Burghardt, which states that homogeneous shear flow data may be used to predict average LCP orientation in nonhomogeneous shear flows. In addition, the good agreement between birefringence and X-ray scattering confirms that, under the conditions of this experiment, birefringence provides an accurate measure of bulk orientation despite spatial variation in the degree of anisotropy along the light path.

The large enhancement of orientation seen at the sidewalls at low flow rates resists easy explanation. The X-ray data presented in Fig. 6 confirm that the enhancement in orientation is real, and not an anomaly associated with a failure of birefringence to reflect the underlying orientation state. Bedford and Burghardt have explored two possible explanations. Both recognize that the two-dimensional nature of the slit flow breaks down due to additional gradients induced by the no-slip condition at the edge of the flow field, leading to effects that should be confined to a region near the side wall comparable with the thickness of the slit flow. The possibility of a transition from tumbling induced by these added velocity gradients [16] proves insufficient, as the added gradients do not fundamentally change the nature of the deformation, so that continued tumbling is expected. On the other hand, Hongladarom and Burghardt [23] have found a significant transverse anisotropy in shear flows, such that the anisotropy observed when viewing along the vorticity direction would be greater than the anisotropy observed when viewing along the gradient direction. Near the side wall, the dominant velocity gradient is normal to the wall. In this region, then, the X-ray beam is actually passing along the vorticity direction of the local shear flow. This should lead to enhanced orientation in this region when viewed through the thickness of the slit flow [18] It is not clear, however, whether these effects can account for the large magnitude of the orientation enhancement.

6.2. Slit-contraction and slit expansion flows

The dramatic increase in orientation in the contraction in our channel flow of lyotropes is reminiscent of that described in a model proposed by Wissbrun [24] for capillary flow of thermotropes. In this model, increases in orientation are induced by a transition to flow aligning behavior

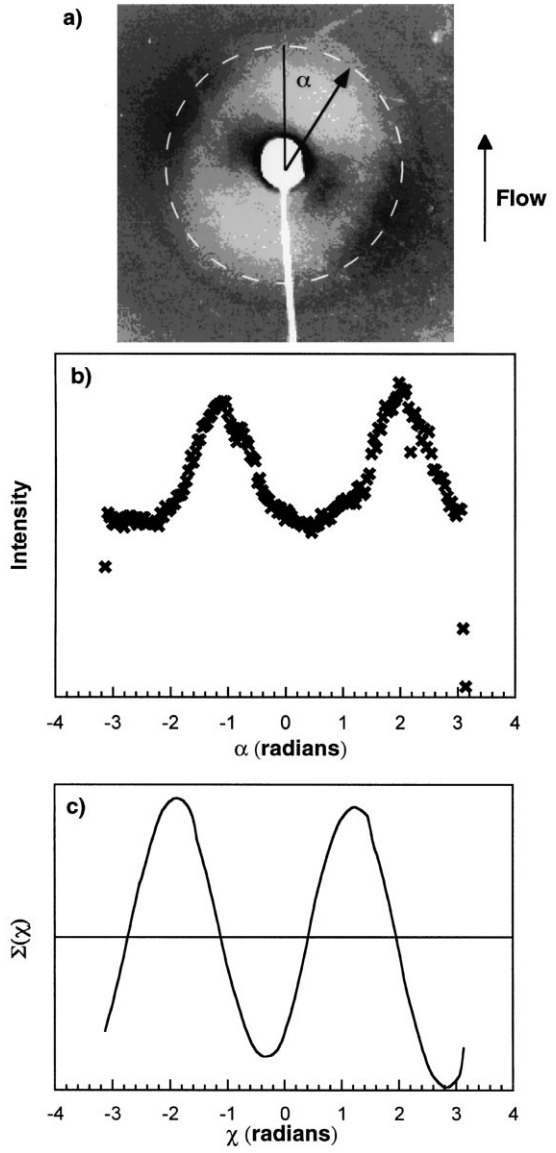

Fig. 8. Method for calculating the amount of rotation out of the downstream direction. (a) Typical scattering image collected away from the centerline, showing rotation of the pattern. (b) Azimuthal intensity distribution; $\alpha = 0$ corresponds to the downstream direction. (c) Intensity sum calculated from Eq. (12) showing the four angles at which $\Sigma(\chi)$ vanishes. Based on this pattern, we conclude that the average LCP orientation is rotated 25° away from the downstream direction.

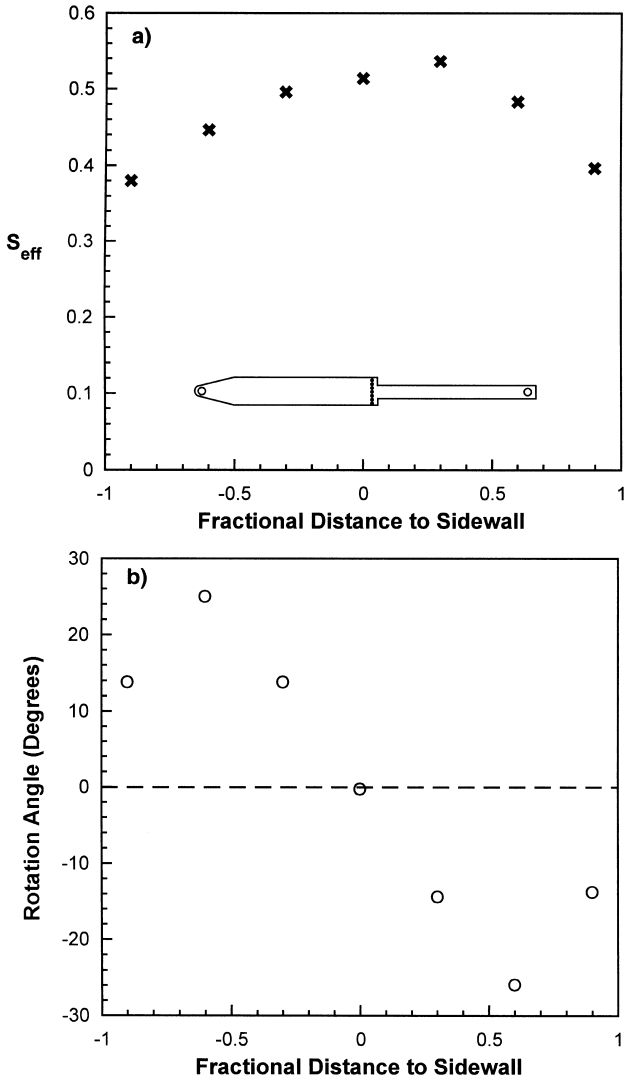

Fig. 9. Orientation as a function of cross-channel position in contraction flow at 1.0 ml.min^{-1}. Data were taken 0.75 cm upstream of the contraction. (a) X-ray scattering orientation parameter (✖). (b) Rotation angle (○). Filled circles on the schematic of the flow field indicate positions at which data were taken. Positive values of the rotation angle denote counter-clockwise rotation.

due to the extensional nature of the contraction flow near the capillary entrance. The subsequent loss in orientation is explained in terms of a gradual transition from flow aligning to tumbling behavior as shear strain accumulates in the straight channel downstream of the contraction. In general terms, these phenomena are borne out in our data.

Bedford and Burghardt [18] also appealed to a transition from tumbling to flow alignment to explain enhancements in orientation induced by contractions in slit flow. However, as discussed earlier, the extension is only a modest perturbation to the dominant shearing gradients in these slit contraction flows, except right at the midplane. On the basis of the calculations in Fig. 2, we propose that significant increases in orientation can occur even in the absence of a transition to an extension-induced flow-aligned state. Since any amount of 'favorable' extension acts to pull tumbling director orbits into the shear plane, there will be a significant orienting effect as misaligned domains are removed, leading to a 'tighter' distribution of director orientation relative to the unperturbed tumbling case. The potential for improvement is significant, since Hongladarom and Burghardt demonstrated that there is greater relative misalignment of orientation out of the shear plane than within the shear plane [23]. As postulated by Bedford and Burghardt [18], only a discrete fraction of the flow near the midplane experiences a transition from tumbling to flow alignment, thus contributing

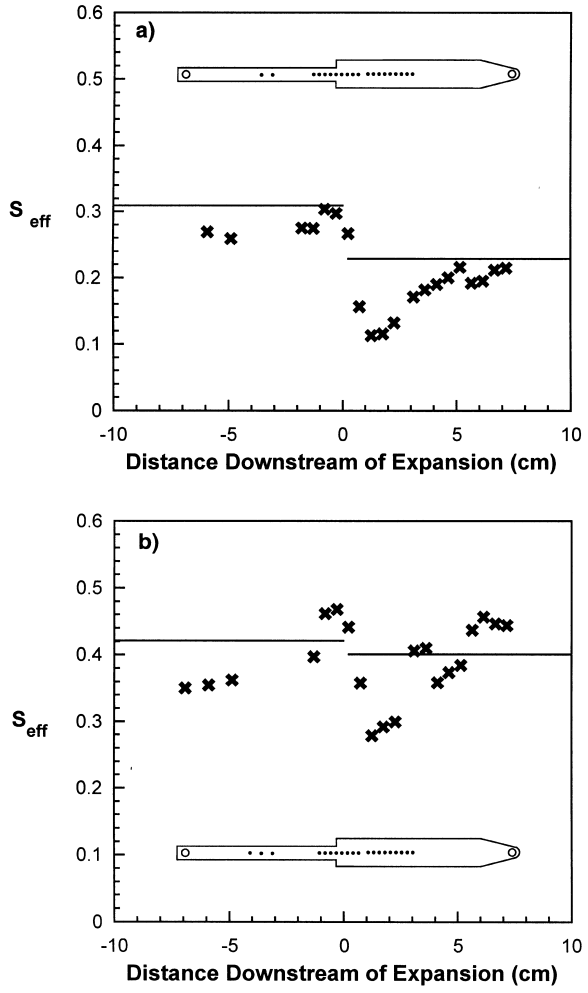

Fig. 10. Centerline orientation in expansion flow for flowrates of (a) 0.1 and (b) 1.0 ml.min^{-1}. Filled circles on the schematic of the flow field indicate positions at which data were taken. Lines denote predictions of orientation in inhomogeneous shear based on flow rate alone.

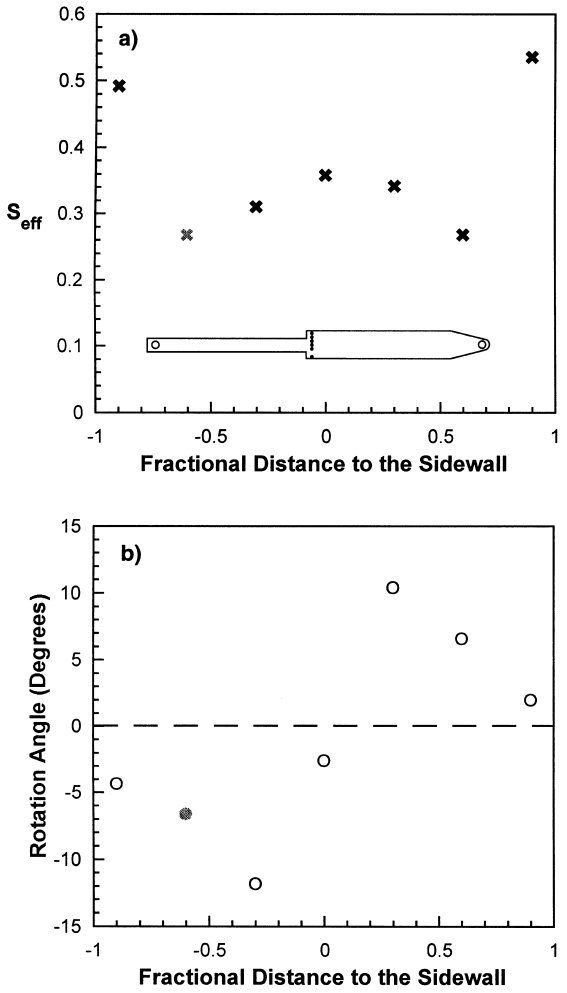

Fig. 11. Orientation as a function of proximity to the sidewall 0.75 cm downstream of the expansion for flowrate of 1.0 ml.min^{-1}. (✖) X-ray scattering orientation parameter and (○) rotation angle. Filled circles on the schematic of the flow field indicate positions at which data were taken. Positive values of the rotation angle denote counterclockwise rotation of the scattering pattern. Shaded symbols represent missing data point, assuming mirror symmetry across the centerline.

to an increase in S_{eff}. This made it difficult to rationalize how such a large effect could result from a thin region near the midplane. Conversely, recognizing that orientation enhancement is possible even in those portions of the flow where tumbling persists, it becomes much easier to explain the magnitude of the orientation enhancement observed in Fig. 7.

In the case of expansion flow, similar effects are taking place, but now the superimposed extension acts to *decrease* net orientation along the flow direction, since it stabilizes vorticity alignment and tends to draw tumbling orbits *away* from the shear plane. If such kinematics persisted indefinitely, a high orientation transverse to the flow direction would be produced. However, the imposition of unfavorable kinematics is a transient event, leading to a temporary drop in orientation which recovers once the fluid enters the straight downstream section. Indeed, in both contraction and expansion flows, the kinematic analysis presented earlier provides some guidance as to what happens locally, but it is also necessary to consider the residence time and total strain accumulated as fluid elements pass through regions of varying shear and extension [18].

7. Conclusions

We have demonstrated that X-ray scattering is a viable method for in situ measurement of orientation in channel flows of LCPs. In all situations where direct comparisons were made, we found that the X-ray results agreed with information provided by birefringence methods. Given that X-ray scattering provides a more direct picture of molecular orientation than birefringence in textured and spatially varying optical media, this affirms the conclusions drawn from previous birefringence studies [16–18]. At the same time, X-ray scattering provides a very direct representation of more complex orientation states, and allows the rotation

of orientation away from the downstream direction induced by the convergence and divergence of streamlines to be easily quantified in contraction and expansion flows. This is a significant improvement, since X-ray techniques are not susceptible to anomalies that can influence birefringence data under similar circumstances [17]. Molecular orientation may be strongly enhanced by superimposed extension along the downstream direction in contracting channel flows, and strongly degraded by superimposed extension transverse to the downstream direction in expanding channel flows. These phenomena are explained in terms of stabilization or creation of steady orientation states in tumbling nematics by strong superimposed extension, or by the attraction of tumbling orbits either into or away from the flow direction by more modest superimposed extension. Significant enhancements in molecular orientation may occur even in the absence of an extension-induced transition from tumbling to flow alignment.

Acknowledgements

We gratefully acknowledge financial support from the AFOSR in the form of a MURI project on Liquid Crystals. These experiments were initiated under support of a National Science Foundation Young Investigator Award, grant CTS-9457083. We would also like to thank the staff of DND-CAT at the Advanced Photon Source of Argonne National Laboratory for assistance with the X-ray scattering experiments.

References

[1] Bensaad S, Jasse B, Noël C. Polymer 1993;34:1602.
[2] Blundell DJ, Chivers RA, Curson AD, Love JC, MacDonald WA. Polymer 1988;29:1459.
[3] Heynderickx I, Paridaans F. Polymer 1993;34:4068.
[4] Ide Y, Ophir Z. Polym Engng Sci 1983;23:261.
[5] Jansen JAJ, Paridaans FN, Heynderickx IEJ. Polymer 1994;35:2970.
[6] Joseph EG, Wilkes GL, Baird DG. Polym Engng Sci 1985;25:377.
[7] Pirnia A, Sung CSP. Macromolecules 1988;21:2699.
[8] Sawyer LC, Jaffe M. J Mater Sci 1986;21:1897.
[9] Thapar H, Bevis M. J Mater Sci Lett 1983;2:733.
[10] Weng T, Hiltner A, Baer E. J Mater Sci 1986;21:744.
[11] Zülle B, Demarmels A, Plummer CJG, Kausch H-H. Polymer 1993;34:3628.
[12] Hongladarom K, Burghardt WR, Baek SG, Cementwala S, Magda JJ. Macromolecules 1993;26:772.
[13] Hongladarom K, Burghardt WR. J Rheol 1994;38:1505.
[14] Burghardt WR, Bedford BD, Hongladarom K, Mahoney M. Flow-Induced Structure in Polymers ACS-Symposium Series 1995;597:308.
[15] Hongladarom K, Ugaz VM, Cinader DK, Burghardt WR, Quintana JP, Hsiao BS, Dadmun MD, Hamilton WA, Butler PD. Macromolecules 1996;29:5346.
[16] Bedford BD, Burghardt WR. J Rheol 1994;38:1657.
[17] Bedford BD, Cinader Jr. DK, Burghardt WR. Rheol Acta 1997;36:384.
[18] Bedford BD, Burghardt WR. J Rheol 1996;40:235.
[19] Burghardt WR, Fuller GG. J Rheol 1990;34:959.
[20] Ericksen JL. Arch Rat Mech Anal 1960;4:231.
[21] Mitchell GR, Windle AH. In: Basset DC, editor. Developments in crystalline polymers—2. London: Elsevier, 1988.
[22] Larson RG, Mead DW. Liquid Cryst 1993;15:151.
[23] Hongladarom K, Burghardt WR. Macromolecules 1994;27:483.
[24] Wissbrun KF. J Rheol 1993;37:777.